Measurement of Inherent Particle Properties by Dynamic Light Scattering: Introducing Electrorotational Light Scattering

Bernhard Prüger, Peter Eppmann, Edwin Donath, and Jan Gimsa
Institute of Biology, Humboldt University, Berlin, Germany

ABSTRACT Common dynamic light scattering (DLS) methods determine the size and ζ-potential of particles by analyzing the motion resulting from thermal noise or electrophoretic force. Dielectric particle spectroscopy by common microscopic electrorotation (ER) measures the frequency dependence of field-induced rotation of single particles to analyze their inherent dielectric structure. We propose a new technique, electrorotational light scattering (ERLS). It measures ER in a particle ensemble by a homodyne DLS setup. ER-induced particle rotation is extracted from the initial decorrelation of the intensity autocorrelation function (ACF) by a simple optical particle model. Human red blood cells were used as test particles, and changes of the characteristic frequency of membrane dispersion induced by the ionophore nystatin were monitored by ERLS. For untreated control cells, a rotation frequency of 2 s^{-1} was induced at the membrane peak frequency of 150 kHz and a field strength of 12 kV/m. This rotation led to a decorrelation of the ACF about 10 times steeper than that of the field free control. For deduction of ERLS frequency spectra, different criteria are discussed. Particle shape and additional field-induced motions like dielectrophoresis and particle-particle attraction do not significantly influence the criteria. For nystatin-treated cells, recalculation of dielectric cell properties revealed an ionophore-induced decrease in the internal conductivity. Although the absolute rotation speed and the rotation sense are not yet directly accessible, ERLS eliminates the tedious microscopic measurements. It offers computerized, statistically significant measurements of dielectric particle properties that are especially suitable for nonbiological applications, e.g., the study of colloidal particles.

INTRODUCTION

Dielectrophoresis (DEP) and electrorotation (ER) are related dielectric spectroscopy techniques. They measure the field frequency dependence of single-particle movement induced by AC fields. In DEP, particles in an inhomogeneous field move toward or away from regions of high field strength, depending on their polarizability relative to that of the suspension medium. Dielectric dispersions mediate the frequency-dependent changes of the DEP force. Such dispersions are characteristic for Maxwell-Wagner, Debye, or complex electrochemical charge transfer processes. In principle, information on dielectric particle properties could also be provided by conventional impedance spectroscopy. Nonetheless, several advantages favor single-particle spectroscopy. These methods are independent of solution volume and electrode impedance because the measured effect, particle movement, is caused by the difference in polarizability of external medium and the particle itself. Extremely low particle concentrations can be used, thereby avoiding particle-particle interactions.

In ER, a rotating field induces a dipole moment on the particles that rotates at the same angular frequency. Depending on the frequency-dependent polarizability of the suspension medium relative to that of the particle, medium or particle polarization dominates. The two cases correspond to an induced dipole moment parallel or antiparallel to the field vector. Any dispersion process causes a spatial phase shift between the rotating external field and the induced dipole moment. Depending on the relative polarizability, the interaction of dipole moment and external field then induces a torque, causing individual particle rotation against (antifield rotation) or in (cofield rotation) the rotation direction of the field. The particle rotation speed depends on rotational friction and is typically on the order of one revolution per second. ER spectra are obtained when particle rotation speed and rotation direction relative to the field are measured as a function of the field frequency. The torque and therefore particle rotation are maximized if the relaxation time of the dispersion process and the period of the external field match. Thus the frequencies of ER peaks correspond to the characteristic frequencies of certain dispersion processes. Dielectric properties can be recalculated by applying appropriate dielectric particle models. Multishell spherical, cylindrical, and ellipsoidal models are readily available (Sauer and Schlögl, 1985; Fuhr et al., 1985; Paul and Otwinowski, 1991; Müller et al., 1993; Jones, 1995). The shells and core of these models consist of homogeneous media characterized by their dielectric constants and conductivities. Furthermore, additional dispersions of the media properties were introduced. They are mediated by dispersions of the transmembrane ion transport (Donath et al., 1990), the inhomogeneity of the cytoplasmatic structure (Asami and Yamaguchi, 1992), Debye dispersions of cytoplasmatic proteins (Gimsa et al., 1996), or dispersions of membrane properties due to the limited mobility of mem-

Received for publication 9 September 1996 and in final form 18 December 1996.

Address reprint requests to Dr. Jan Gimsa, Institut für Biologie, Humboldt-Universität zu Berlin, Invalidenstrasse 42, D-10115 Berlin, Germany. Tel.: +49-30-20938494; Fax: +49-30-20938520; E-mail: jan=gimsa@rz.hu-berlin.de.

0006-3495/97/03/1414/11 $2.00

brane-trapped lipophilic ions (Sukhorukov and Zimmermann, 1996).

Despite their principal advantage, microscopic ER measurements are tedious and restricted to the microscopically accessible particle range. Large numbers of measurements on single particles are required for statistical significance. To overcome these drawbacks we introduce electrorotational light scattering (ERLS), a combination of ER and conventional dynamic light scattering (DLS). DLS analyzes the fluctuations of light scattered by suspended particles. An autocorrelation analysis of the light intensity is performed to obtain concise information on the particle movement. The light intensity $I(t)$ for any time t is multiplied by the intensity at an instant τ later, $I(t + \tau)$. Averaging over t leads to the autocorrelation function (ACF) $C(\tau) = \langle I(t)I(t + \tau)\rangle / \langle I(t)\rangle^2$, a function that depends only on the correlation time τ. Generally, the stochastic nature of the particle motion results in a decorrelation of the intensity signal. For example, for pure translational diffusion and a monodisperse suspension a single exponentially decaying ACF is obtained (Berne and Pecora, 1976; Ostrowski, 1993).

ERLS allows the simultaneous registration of the field-induced individual movement of many particles or cells within a population. To apply ERLS to particle rotation, an optical anisotropy of the particles is required. Our ERLS setup uses a single beam–single detector setup to record the ACF of scattered light intensity from suspensions of such particles. The field frequency-dependent particle motion generates field frequency-dependent ACFs. First qualitative results on ERLS measurements have been published recently (Gimsa et al., 1995). They were conducted in a special ER chamber fitted into the cuvette holder of a commercial light-scattering device. In the meantime, a light scattering theory for ERLS (Eppmann et al., 1996) and an optimized ERLS setup have been developed.

In the field of biology ER is a useful method for detecting dielectric property changes of single cells caused by the physiological impact of certain treatments (for reviews see Fuhr et al., 1996; Gimsa et al., 1991a). To test our new method, we used human red blood cells, because their dielectric properties are well known (Pauly and Schwan, 1966; Bao et al., 1993; Gimsa et al., 1996). Like most biological cells, these cells show spectra with two major peaks, an antifield rotation peak in the kilohertz range and a cofield peak in the megahertz range. The processes generating these peaks are related to membrane polarization and the dispersion of ohmic conductivity-dominated polarization, respectively. The two peaks are especially sensitive to membrane capacitance and cytoplasmic conductivity. When the two ER peaks are sufficiently separated, in the peak range the torque dependence on field frequency, f, is proportional to the Lorentzian term, $(f/f_c)/(1 + (f/f_c)^2)$, where f_c stands for the characteristic frequency of the respective dispersion process (Fuhr et al., 1985; Pastushenko et al., 1985). In addition, red cells possess significant optical structures. Nystatin was applied to induce changes in ER behavior, to be followed by ERLS. It induces a loss of cytoplasmatic ions, which can be followed on single cells as a change in their dielectric properties (Gimsa et al., 1994). This model system allows us to discuss limitations and new possibilities of ERLS and to test a theory for extraction of ER spectra from the ACFs.

MATERIALS AND METHODS

Measuring chamber

For ER measurements by DLS we designed an optically transparent chamber (Fig. 1 *A*). The coverslips of the chamber could be removed for cleaning. Four 90° phase-shifted signals were applied to four electrodes, inducing a vertically rotating field in a plane perpendicular to the optical axis. The distance of two opposing electrodes was about 1.4 mm. The electrodes were driven by a home-made four-channel power amplifier by symmetrical square-wave signals with a maximum amplitude of 25 V_{pp}. At

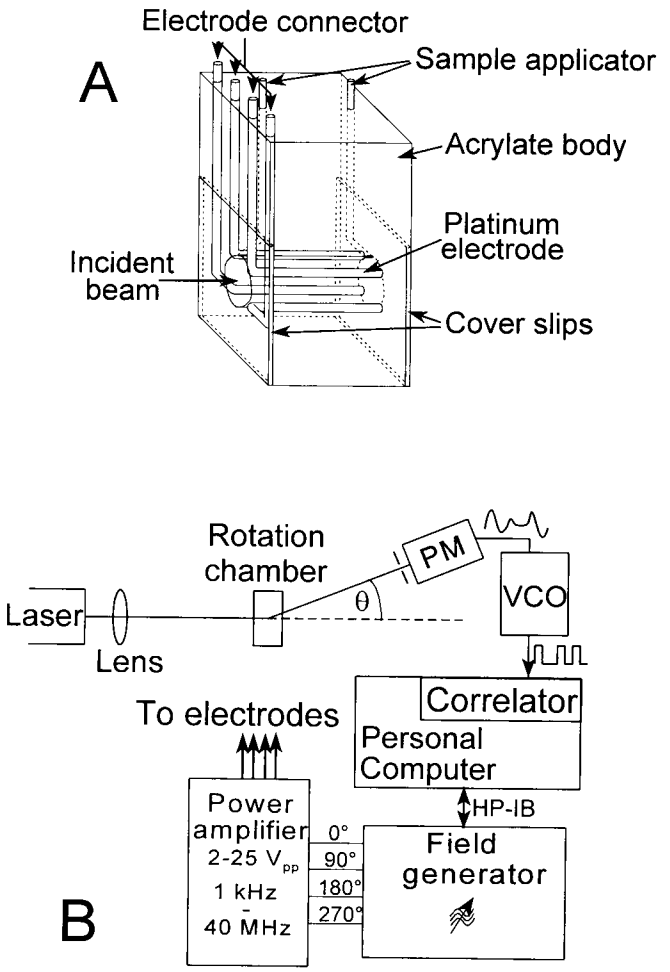

FIGURE 1 Experimental setup for ERLS measurements. (*A*) Design of the measuring chamber. The measuring volume is given by a cylindrical drill hole of 5 mm length and a diameter of 2 mm. The platinum wire electrodes (diameter 0.8 mm) partially project into the measuring volume. (*B*) The measuring chamber was illuminated by a laser beam 100 μm in diameter. Scattered light intensity was detected through a pinhole by a photon multiplier (PM) at the detection angle θ. The analog PM signal was processed by a voltage-controlled oscillator (VCO) and fed into the correlator. The computer containing the correlator card also drove the four-phase-field generator via the Hewlett-Packard interface bus (HP-IB).

a driving voltage of 16 V_{pp}, an antifield peak rotation speed of approximately 2 s^{-1} was measured microscopically for control cells.

ERLS device

The ERLS device consisted of the components depicted in Fig. 1 *B*. A 10-mW HeNe laser (λ = 632.8 nm) was used. All optical components were arranged on an optical bench so that they would be freely accessible. The chamber was aligned by an *x-y* stage relative to the laser beam to ensure optical detection from its center. To observe the scattered light with and without particles and to approximate homodyne detection, a screen in the detection plane was used. Homodyne detection is essential for minimizing the influence of particle flows on the detected fluctuation signal. During measurements, a long-distance microscope (model K2; ISCO-OPTIC GmbH, Göttingen, Germany) enabled us to check the chamber for undesired flows or bubbles.

The analog light intensity signal detected by a photon multiplier (model H5773–01; Hamamatsu Photonics Deutschland GmbH, Herrsching, Germany) through a 100-μm pinhole was transformed into a digital pulse signal by a home-made voltage-controlled oscillator. The autocorrelation analysis of the digital signal was performed by a correlator card (BI-9000AT; Brookhaven Instruments, Holtsville, NY). Field frequencies and amplitudes of a measuring protocol could be programmed to a personal computer containing the correlator card. The computer also drove the field generator (pulse generator HP8130A; Hewlett-Packard, Rockville, MD).

ERLS measurements

Previous measurements and theoretical considerations have indicated that the detected rotation effect is maximized near an effective scattering angle θ = 10° (Gimsa et al., 1995; Eppmann et al., 1996). To reduce the number of experimental parameters to be considered, the angle was fixed at θ = 10° (see also Discussion). The effective scatter volume can be approximated from chamber length and beam diameter to be about 0.04 mm^3. At a cell concentration of 0.02% (v/v), this corresponds to a mean particle number of about 80. The sample time of the correlator, $\Delta\tau$, denoting the smallest decay step in the ACF, was set to 5 ms. With its 236 linearly spaced channels, the correlator allowed a maximum correlation depth of 1.18 s. The 5-ms sample time provided a temporal resolution high enough for the analysis of individual particle rotation up to the peak rotation speed. Furthermore, the correlation depth was still long enough to observe the slow diffusional decorrelation without field-induced motion. ERLS frequency spectra were measured over four decades of the external field frequency at approximately 2:1 frequency steps. To allow measurement of complete ERLS spectra within 6 min, a correlator run time of 20 s was used for each measuring point.

Measuring solutions

For measurements, human red blood cells were suspended in an isotonic 300 mOsmol sucrose solution containing 1 mM phosphate buffer (pH 6.8). Unless stated otherwise, a hematocrit of 0.02% (v/v) was used. The conductivity of the suspension was checked after every measurement. It was usually about 10 mS/m. To perform nystatin measurements, various amounts of a stock solution (5 mM nystatin in dimethylformamide) were added to the solution before cell suspension (for details see Gimsa et al., 1994). The suspension was injected into the measuring chamber by a syringe via tubes. All measurements were carried out at a room temperature of 23°C.

RESULTS

Influence of field-induced cell rotation on the ACF

The effect of ER on the ACF was measured at a driving voltage of 16 V_{pp} and a frequency of 150 kHz. This frequency is close to the antifield peak frequency of the cells. Microscopic observation revealed that ER oriented the oblate cells. They rotated at about 2 revolutions/s around their short axis. Fig. 2 clearly shows that induced rotation resulted in a decay of the ACFs approximately 10 times steeper than the control. Nonreproducible fluctuations remained on the baseline level calculated from the square of the averaged intensity. These fluctuations had a higher rate than those measured for the control without field. The inset in Fig. 2 shows that the initial part of the ER-ACFs is not an exponential decay function. Therefore, a simple interpretation (as in the case of diffusion) is not possible. Nevertheless, for given field conditions and cell concentration, the initial decay of the ACFs was fairly reproducible. We found that the time necessary for the ACF to decay to a given level (e.g., $C(\tau) - 1 = 0.75$) decreases with the induced cell rotation speed. To consider the influence of different experimental parameters on the ACFs obtained by ERLS, we used the reciprocal of the 0.75 decay time of an ACF ($1/\tau_{75}$) as a measure of the ER speed.

Without field, a large error range for the ACFs was found. This was due to the short run time (20 s). On averaging several ACFs, a smoothly decaying mean ACF was obtained (Fig. 2). It exhibited a local minimum at a correlation time of about 1.5 s. The minimum (outside the range presented in Fig. 2) was below the baseline. This behavior can only be explained by a partially heterodyne detection, which could not be avoided with our complex chamber structure.

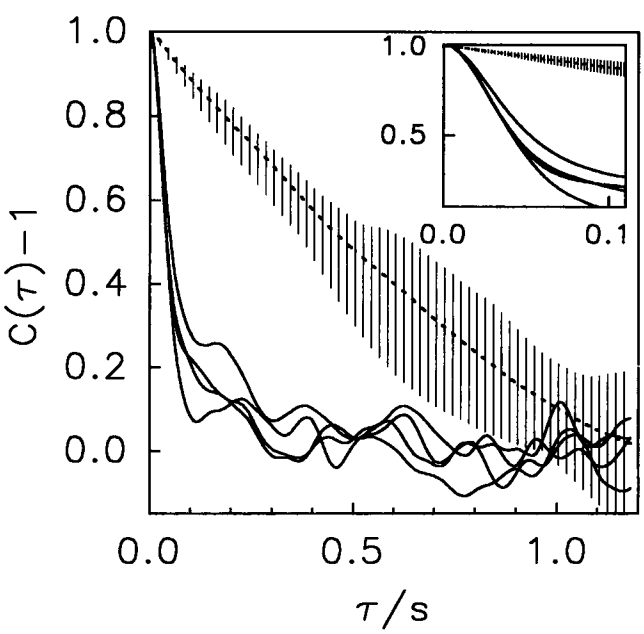

FIGURE 2 Influence of ER on the ACF of a red blood cell suspension at an external medium conductivity of 10 mS/m. The baseline-substracted ACFs were normalized to unity at τ = 0. The control curve (*dashed lines*) represents the average of eight ACFs obtained from control cells without field. Maximum and minimum values of all control ACFs are presented as error range. For clarity, only four ACFs are shown in the presence of a rotating field of 150 kHz.

Influence of cell concentration on ER-decorrelation of the ACF

To find an optimal cell concentration for ERLS, we made repetitive measurements of the $1/\tau_{75}$ values at different cell concentrations. Results for field frequencies of 25 kHz and 200 kHz and without field are presented in Fig. 3. It can be seen that the reproducibility and the sensitivity (values with field compared to those without field) are comparably good above 0.005%.

But sensitivity is not the only criterion. The cell concentration must be low enough to avoid aggregation or electrical and hydrodynamic cell-cell interactions. Furthermore, for concentrations of 0.08% and above, multiple scattering increased. It could be observed that for such concentrations the zero beam was significantly weakened. To obtain high sensitivity for ER detection at low deviations, we therefore used 0.02% for further experiments. This concentration ensured high reproducibility of the $1/\tau_{75}$ values, low cell-cell interaction, and low multiple scattering.

Correlation of the $1/\tau_{75}$ criterion with cell rotation speed

To test whether $1/\tau_{75}$ is a reliable quantitative measure of cell rotation speed, we varied the rotation speed by changing the field frequency and the field strength (Fig. 4). Rotation speed varies with the square of the applied field strength and a Lorentzian frequency dependence. Changing the frequency around the antifield peak alters the rotation speed without affecting the overall Joule heating, leaving possible thermal convections in the ERLS chamber unchanged. In Fig. 4 *A*, $1/\tau_{75}$ values are plotted for six different field frequencies. For each frequency, four different driving voltages were used. A quadratic scaling of the abcissa was used because of the known quadratic field strength dependence. As expected, the $1/\tau_{75}$ increase with driving voltage was stronger for frequencies closer to the peak.

The correlation of the $1/\tau_{75}$ criterion with the rotation speed is presented in Fig. 4 *B*. Relative rotation speeds were calculated, taking the speed at the characteristic frequency and a driving voltage of 16 V_{pp} as unity. The characteristic frequency was obtained according to the model of Gimsa et al. (1996) to be 140 kHz at the medium conductivity of 9.6 mS/m. All $1/\tau_{75}$ values obtained with field are clearly above the control for pure diffusion. Above a relative rotation of 0.4, these points fit to a linear dependence with a correlation

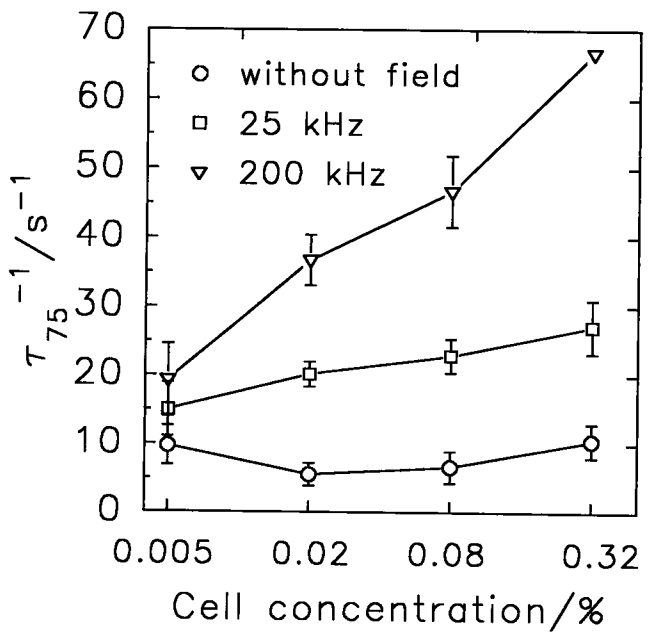

FIGURE 3 Concentration dependence of $1/\tau_{75}$ values for red blood cell suspensions under the influence of a rotating field. Control values without field and field frequencies of 25 kHz and 200 kHz are presented. Each point represents six measurements.

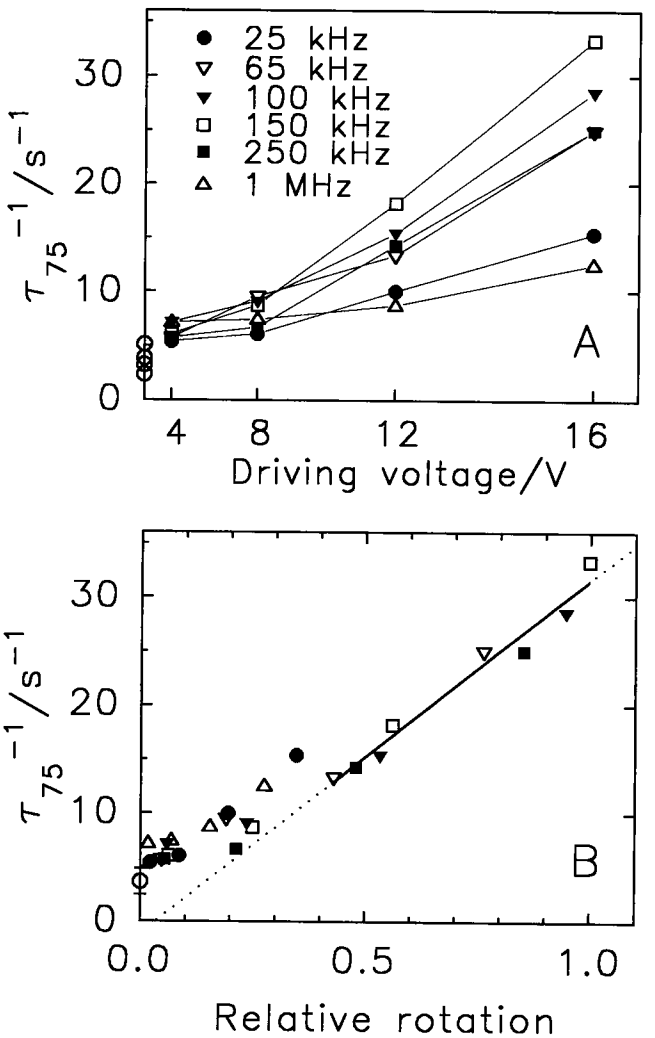

FIGURE 4 Influence of ER on the $1/\tau_{75}$ criterion. (*A*) Dependence of $1/\tau_{75}$ values on driving voltage at different field frequencies. (*B*) $1/\tau_{75}$ values plotted over relative rotation speed. The relative rotation speed was recalculated from the theoretical dependence on field strength and frequency (see text). The line represents a linear regression for a relative rotation speed higher than 0.4.

coefficient of 0.98. This behavior proves that ERLS is sensitive for the detection of ER peaks, where the highest rotation speeds occur. For relative rotations below 0.1, the increase in induced rotation cannot be resolved. Obviously, the field induces particle motions other than rotation that lead to a decorrelation adding to that caused by Brownian motion. Above 0.1 it can be seen that fields that do not efficiently induce cell rotation (25 kHz and 1 MHz) yield higher $1/\tau_{75}$ values, although they induce a relatively low rotation.

ER spectra measured by ERLS

Fig. 5 compares different criteria to obtain ERLS spectra from ACF measurements. For each frequency six ACF recordings were summarized. A $1/\tau_{25}$ criterion and an initial decay criterion derived from the same ACFs are plotted in Fig. 5, *D* and *C*, in addition to the $1/\tau_{75}$ criterion (Fig. 5 *B*). The initial decay criterion is the averaged decay rate of the normalized ACFs within the first 30 ms. The short (30-ms) interval ensured that the nonreproducible fluctuations of the ACFs did not affect the initial decay values. From measurements of the field strength dependence, this criterion was found to increase approximately with the square of cell rotation speed (see also Discussion and Fig. 9 *B*).

To facilitate the interpretation of the different ERLS criteria, a comparison with theoretical curves is provided (Fig. 5 *A*). The latter are calculated from the dielectric cell model of Gimsa et al. (1996). For the direct comparison of the ERLS results with the theoretical ER spectrum, the imaginary part of the Clausius-Mossotti factor (Fig. 5 *A*, *solid curve*) was transformed in different ways to obtain theoretical ERLS spectra (Fig. 5, *B* and *C*, *solid curves*; for further details see Discussion). All ERLS spectra clearly exhibit a maximum in the frequency range of the antifield ER peak. A slight depression, most obvious for the $1/\tau_{25}$ criterion (Fig. 5 *D*), can be seen at 100 kHz. Because ERLS is not sensitive to the sense of rotation, spectra do not show the reversal of rotation above 2 MHz. After a minimum at around 2 MHz, the values increase again, exhibiting a small plateau around 12 MHz. Microscopic observations of the cells in parallel to ERLS measurements showed that cells reorient around this frequency. Below 12 MHz the oblate cells always rotated around their short axis. After reorientation they rotated perpendicular to that axis. Another difficulty was that only the low-frequency flank of the cofield peak (theoretically expected at 33 MHz) could be measured, because 25 MHz was the highest frequency that could be reached by our device. Because of these difficulties, we decided to focus on the interpretation of the antifield peak. The characteristic frequency of this peak was extracted by nonlinear regression in the range from 12.5 kHz to 1 MHz (Fig. 5, *B* and *C*, *dashed lines*). For the $1/\tau_{75}$ data, a Lorentzian function consisting of a scaling factor and an offset was used. Similarly, the initial decay values were fitted, except that a quadratic Lorentzian function was ap-

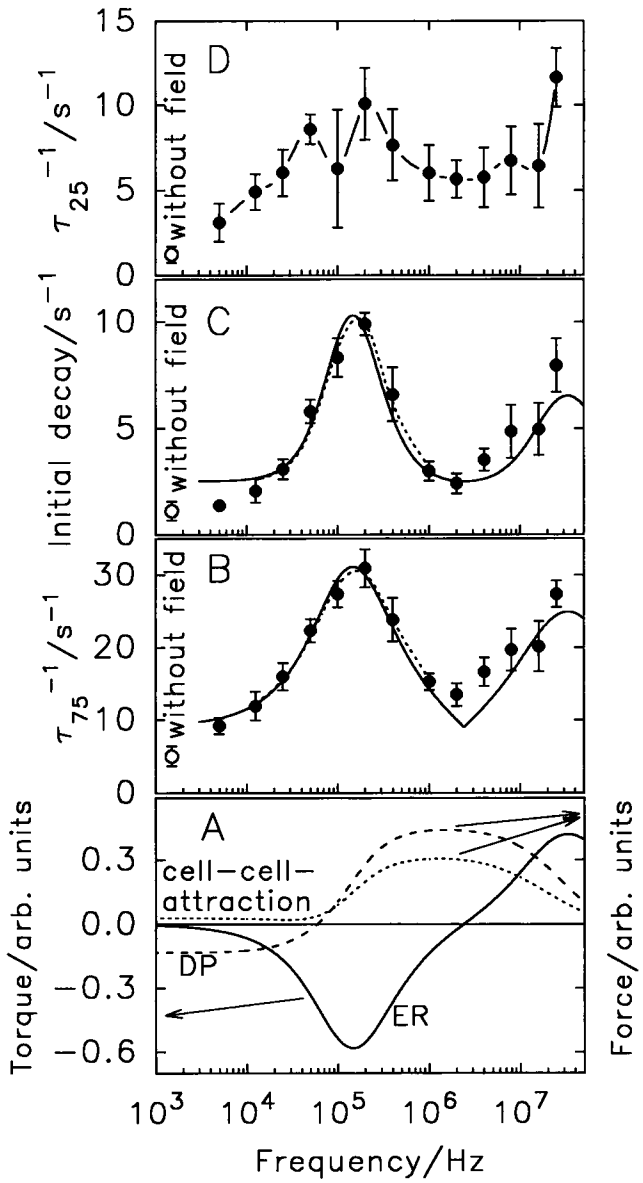

FIGURE 5 Comparison of theoretical frequency spectra obtained from the dielectric cell model (*A*) and ERLS measurements (*B*, *C*, and *D*). Every point in *B*, *C*, and *D* represents data obtained by the same six ACF measurements. (*A*) Solid line: ER spectrum given as the frequency-dependent imaginary part of the Clausius-Mossotti factor of the cell model at a medium conductivity of 10 mS/m (see text). Dashed line: The real part of the Clausius-Mossotti factor decribing the frequency dependence of the dielectrophoretic force, i.e., the force acting on a cell due to field inhomogeneities within the chamber. Dotted line: The square of the absolute value of the Clausius-Mossotti factor describing the frequency dependence of the cell-cell attraction force. (*B*) ERLS spectrum of red blood cells. The points represent data obtained by the $1/\tau_{75}$ criterion. The dotted line represents a nonlinear fit of all points of the antifield peak range (see text). The solid line is the theoretical spectrum of the dielectric cell model transformed as described in the text. (*C*) Data obtained by the initial decay criterion. The dotted line represents a nonlinear fit of the antifield peak. The solid line is a transformation of the theoretical spectrum according to the initial decay criterion (see text). (*D*) Data obtained by the $1/\tau_{25}$ criterion. The solid line is a spline curve. The influence of dielectrophoretic effects is clearly visible at 100 kHz (see Discussion).

plied. Values of 160 and 162 kHz for the position of the antifield peak were found from the two criteria.

ERLS spectra measured on red blood cells under the influence of nystatin

The time dependence of ERLS spectra under the influence of nystatin was followed in the antifield peak range from 25 kHz to 1 MHz. In Fig. 6 the spectra of runs without nystatin (control cells) as well as for 10 μg/ml and 20 μg/ml nystatin are shown. After cell suspension for every nystatin concentration, the measurements were repeated three times at 10-min intervals. The measuring protocol consisted of the detection of a control ACF without field 2 min after chamber filling. The frequency dependence of the ACFs was then measured at six frequencies, starting at 1 MHz. At each frequency the ACF was recorded for 20 s, starting 2 s after the rotating field was switched on. Using this protocol, individual spectra could be measured within 3 min. The whole measurement was carried out within 120 min on the same blood sample. ERLS spectra were obtained from the $1/\tau_{75}$ criterion (Fig. 6) and from the initial decay criterion (not shown). Fits of the spectra according to the procedures described above yielded the characteristic frequency, f_c, of the antifield peak, as well as a scaling factor. The offset of all measurements did not vary significantly; it was not considered further. Changes of the peak rotation speed were derived from changes of the scaling factor relative to that of the control. In Table 1, the fitted peak frequencies and peak heights are compiled for both the $1/\tau_{75}$ and the initial decay criteria.

Control spectra showed no significant shift of characteristic frequencies f_c or rotation speed within 35 min. Under the influence of nystatin, a decrease in f_c was found. For 10 μg/ml nystatin, the decrease started only after 12 min. Also for this concentration, the spectrum at 12 min reproducibly indicated a higher rotation speed than at 2 min. However, microscopic observation proved that this was not the case, and under the influence of nystatin, the rotation speed and frequency decreased in a continuous way. We observed that after application of nystatin, cells underwent shape changes that obviously changed their scattering properties. Control cells were mainly biconcave (normocytes) with microscopically visible details at their periphery. After nystatin application, cells clearly became smoother. Within 10 min they changed to stomatocytes and then developed peripheral optical inhomogeneities. These processes are also related to cell shrinkage. Exposed to our measuring solution, the control cells shrank to about 70% of their physiological volume within 30 min. Shrinkage was strongly enhanced by nystatin (Gimsa et al., 1994).

When nystatin was applied at 20 μg/ml, a much faster decrease in rotation speed could be observed. For this reason the $1/\tau_{75}$ value and the initial decay value decreased significantly during registration of the first ERLS spectrum. After 4 min the values became almost frequency independent. They could no longer be interpreted as ER spectra. Fitted peak frequencies in Table 1 are therefore given in brackets only for the sake of completeness.

DISCUSSION

ACFs for control cells without rotating field

Human red cells have an average volume of 97 μm^3 (Engström et al., 1992). This corresponds to the volume of a sphere of 5.7 μm diameter. Interpretation of the ACF by a single exponential decay under the assumption of homodyne detection (Berne and Pecora, 1976) led to a spherical hydrodynamic diameter of 3.1 μm. The assumption of pure heterodyne detection would halve the calculated diameter. Hence the control ACF is fairly consistent with particle size,

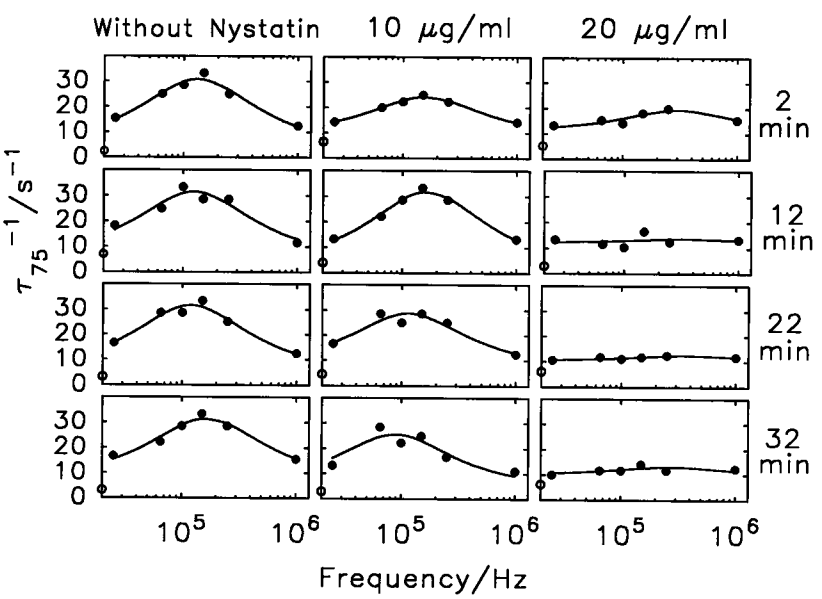

FIGURE 6 Time dependence of ERLS spectra for cells in measuring solution without nystatin and under the influence of two different nystatin concentrations. At the indicated time after suspension, spectra were recorded within 3 min. Empty circles represent $1/\tau_{75}$ values of the ACFs without rotating field. The medium conductivity was 9.5 mS/m.

TABLE 1 Time dependence of the antifield peak parameters f_c and peak height, on nystatin concentration obtained from two different ERLS criteria

	Antifield peak expressed by f_c/kHz; peak/s^{-1}					
	$1/\tau_{75}$ criterion			Initial decay criterion		
Time after suspension	Without nystatin	10 μg/ml	20 μg/ml	Without nystatin	10 μg/ml	20 μg/ml
2 min	134 ; 25	157 ; 15	(304) ; 8	136 ; 5.3	147 ; 2.8	(264) ; 1.6
12 min	125 ; 24	163 ; 27	(367) ; 1.5	120 ; 6.5	146 ; 4.4	(522) ; 0.3
22 min	119 ; 25	114 ; 20	(370) ; 2	135 ; 5.4	118 ; 3.3	(103) ; 0.2
32 min	164 ; 23	89 ; 20	(269) ; 3	144 ; 6	96 ; 2.6	(302) ; 0.3

although the size of human red cells is at the upper limit for reliable radius detection by DLS.

Red blood cells possess a nonspherical, oblate shape. Therefore rotational diffusion may cause two general types of motion. Rotation around the short axis would not change the effective form factor for a cell with a homogeneous optical structure. Any other rotation results in tumbling and a change in the form factor with time. Such changes result in a steeper decay of the ACF and consequently in a cell radius miscalculation.

Effect of field orientation on ERLS

Field-induced orientation of the cells changes their optical form factor. Field orientation of cells is usually investigated in linear AC fields. Its frequency behavior depends on the external conductivity. At our conductivity, Miller and Jones (1993) described reorientation of the short axis of red blood cells from parallel to perpendicular to the field when the field frequency exceeded 20 MHz. Our microscopic observation in the ERLS chamber showed that the cells rotate around their short axis in the frequency range from 5 kHz to 8 MHz. This axis is oriented perpendicularly with respect to the plane of field rotation and parallel to the laser beam in our optical setup. In the range of 8–12 MHz, reorientation was observed. Above 12 MHz the cells rotated around a long axis. Thus observations in linear and rotating AC fields are contradictory. The reason is not yet well understood. Most probably, hydrodynamic phenomena that are unique for ER are responsible.

The phenomenon of cell reorientation in rotating fields was not further investigated because it appeared beyond the antifield rotation peak. It is clear that the degree of orientation depends on the field strength. For smaller field strengths a stronger tumbling must be expected. Microscopically, a strong orientation could already be observed at the lowest driving voltage of 4 V. For the optical model, orientation means the disappearence of tumbling and therefore the loss of two degrees of freedom for the rotational diffusion.

Theoretical description of the ACF

A first theoretical approach for the description of ERLS was published by Eppmann et al. (1996). It assumes a spherical model of radius R with a single optical inhomogeneity at radius r_s (Fig. 7). For homodyne detection the solution for the ACF of this model undergoing translational and rotational diffusion in parallel to the deterministic ER is given by

$$C(\tau) = 1 + |g_t(\tau)g_\varphi(\tau)g_r(\tau)|^2, \tag{1}$$

where the τ-dependent term is factorized, because the three movements are independent (Pecora, 1985). The factors are given by

$$g_t(\tau) = \exp\left(- D_t\left(\frac{4\pi n}{\lambda}\sin(\theta/2)\right)^2 \tau\right)$$

with

$$D_t = \frac{kT}{6\pi\eta R}, \tag{2}$$

describing the translational diffusion,

$$g_\varphi(\tau) = J_0\left(-\frac{4\pi n}{\lambda} r_s \sin\theta\right) + 2\sum_{m=1}^{\infty} \exp(-(2m)^2 D_\varphi \tau) J_{2m}\left(-\frac{4\pi n}{\lambda} r_s \sin\theta\right) \tag{3}$$

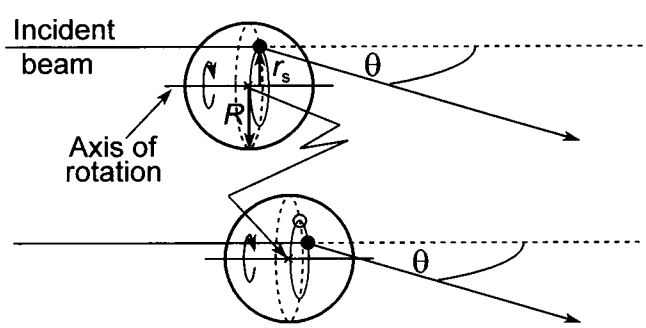

FIGURE 7 Spherical optical particle model simultaneously undergoing translational and rotational diffusion, as well as the deterministic field-induced rotation. For rotational diffusion, only the component around the ER axis was considered.

with

$$D_\varphi = \frac{kT}{8\pi\eta R^3}$$

describing the rotational diffusion and

$$g_r(\tau) = J_0\left(-\frac{4\pi n}{\lambda} r_s \sin\theta \sin(-\omega\tau/2)\right) \quad (4)$$

describing the deterministic ER. J_n denotes the nth-order Bessel function, θ the scattering angle, k Boltzmann's constant, T the absolute temperature, n the refractive index of the suspension medium, η the medium viscosity, and ω the angular speed of field-induced rotation. For the particle ensemble, a Gaussian distribution of the individual rotation speeds was easily introduced by averaging the ACFs of such a distribution. The influence of a distribution of the optical properties can be described when a spatial distribution for the position of the optical inhomogeneity within the particle ensemble is assumed. In this case the ACF of the ensemble was calculated by averaging over a distribution of individual positions of the optical inhomogeneities.

For calculations, the red cells were assumed to be spheres of a radius of 3 μm rotating at the speed measured microscopically in the center of our chamber. Viscosity, refractive index, and temperature were assumed to be 10^{-3} Pa*s, 1.33, and 295 K, respectively. To obtain an appropriate model, the theoretical initial decay of the ACF was compared to the experimental decay. The particle rotation speed at different field strengths was measured microscopically. The position of the optical inhomogeneity in the model was varied. We found that the initial decay of experimental and theoretical ACFs corresponded for various particle rotation speeds when r_s was assumed to be about 1 μm. This correspondence could also be found when the ERLS criteria were applied to theoretical ACFs (see below).

The model predicts that major ACF maxima should exist at correlation times corresponding to multiples of the revolution period (Fig. 8; Eppmann et al., 1996). This should be true, even when a distribution width for the rotation speed comparable to that found in microscopic measurements (7%, compare to Georgiewa et al., 1989) was assumed (Fig. 8 *A*). Only when a larger distribution than that found in experiments (15%) is assumed, the first major maximum declines below the values of the minor maxima (Fig. 8 *A*; compare to Fig. 2). Even then, distinct minima remain that could not be found experimentally. For a better description, a spatial distribution of the scatterer positions was introduced. A homogeneous distribution of the scatterer position on a concentric spherical surface within the spherical particle was assumed. The ACFs for different radii of the spherical surface were calculated (Fig. 8 *B*). As can be seen for such a distribution, the major maxima are little affected. For a spherical radius of 1 μm, the first major maximum of the ACF at τ = 1 s even increased. This is caused by the reduced influence of the rotational diffusion. The sharp minima disappeared. A combination of speed and spatial distribution was not calculated, because of insufficient computing capacity.

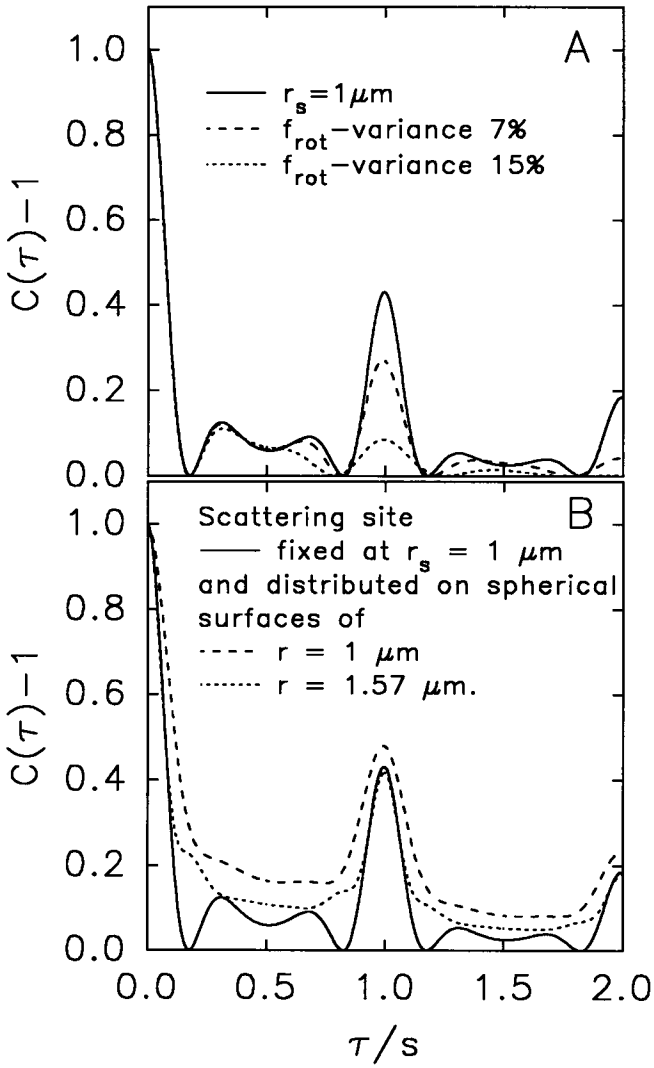

FIGURE 8 Theoretical ACFs for particle ensembles with different distributions of the particle properties. The solid line represents a homogeneous ensemble of spherical particles of 3 μm radius, at a particle rotation frequency of 1 s^{-1} for r_s = 1 μm and a scattering angle of 10°. All spectra were calculated from Eq. 1. (*A*) Effect of a Gaussian distribution of the particle rotation frequency within the ensemble. Variations of 7% and 15% around the mean frequency of 1 s^{-1} are considered. (*B*) Effect of a distribution of the position of the particles' optical inhomogeneities. Only distributions on concentric spherical surfaces within the particles were considered. Homogeneous distribution of the optical inhomogeneity on surfaces of two different radii were assumed. A radius of 1.57 μm corresponds to an average r_s of 1 μm.

Despite the complexity of the optical cell structure, we think that there are several other reasons for discrepancies between experimental and theoretical ACFs, e.g., partially heterodyne detection of field-induced translational movement of the particles (e.g., DEP; see below). Such movement as well as field-induced and thermal medium convections may cause fluctuations in the ACF around the baseline (see Fig. 2). In result, we were not able to extract the

rotation speed from the position of the extrema found in the experimental ACFs.

As can be seen in Fig. 8, the range of the initial decay of the ACF is little affected by the distributions. Because we only interpret the initial part of the experimental ACFs, we neglected the distributions considered above. A simple model with r_s set to 1 μm was applied to simplify further considerations.

Scattering angle

An optimal angle for the detection of ERLS can be estimated from our simple particle model. At this angle the ACF decay caused by particle rotation should dominate the ACF. To find the optimal angle, we compared the influence of the diffusional terms ($|g_t g_\varphi|^2$) and the ER term ($|g_r|^2$) on the theoretical ACF (Eq. 1). For an increasing value of the scattering angle, θ, starting at very low angles, the zero-order Bessel function of g_r and therefore the ACF minima will reach zero for

$$\frac{4\pi n}{\lambda} r_s \sin\theta \geq 2.4.$$

In our model (r_s = 1 μm) this is the case around 5°, the lower limit of θ for sensitive ERLS detection. With increasing θ the diffusion terms overwhelm the deterministic rotation. Therefore, the decorrelation contribution of these terms ($|g_t g_\varphi|^2$) to the ACF should be weak enough to leave the $|g_r|^2$ contribution detectable. A universally valid criterion for such a condition can hardly be found, because it would depend not only on θ but also on the optical and diffusive particle properties, as well as on the induced rotation speed. Provided that (for increasing angles) $|g_t g_\varphi|^2$ remains larger than 0.1 at the correlation time (τ) corresponding to one particle revolution, $|g_r|^2$ can significantly contribute to the ACF decorrelation. For 1 revolution/s and a particle radius of 3 μm, $|g_t g_\varphi|^2$ is 0.1 at about 16°. Accordingly, θ was fixed between these limits, at 10°, for experiments.

Criteria for the particle rotation speed

From both experiments and model considerations, we found that interpretation of the initial decay range of the ACF may yield a reliable measure for the rotation speed of the particles. Two simple kinds of criteria can be imagined: to interpret the time needed for a certain decay of the ACF (decay-level criterion; see Fig. 5, *B* and *D*), or to measure the decay within a certain correlation time (initial decay criterion; see Fig. 5 *C*). In Fig. 9 both criteria are applied to theoretical ACFs for particle rotation frequencies of up to 2 revolutions/s. To ensure that the decay-level criterion increases with increasing particle rotation speed, it was expressed by inverse correlation time. Fig. 9 *B* shows that these decay-level criteria result in an almost linear dependence on the particle rotation rate. Only the 90% criterion

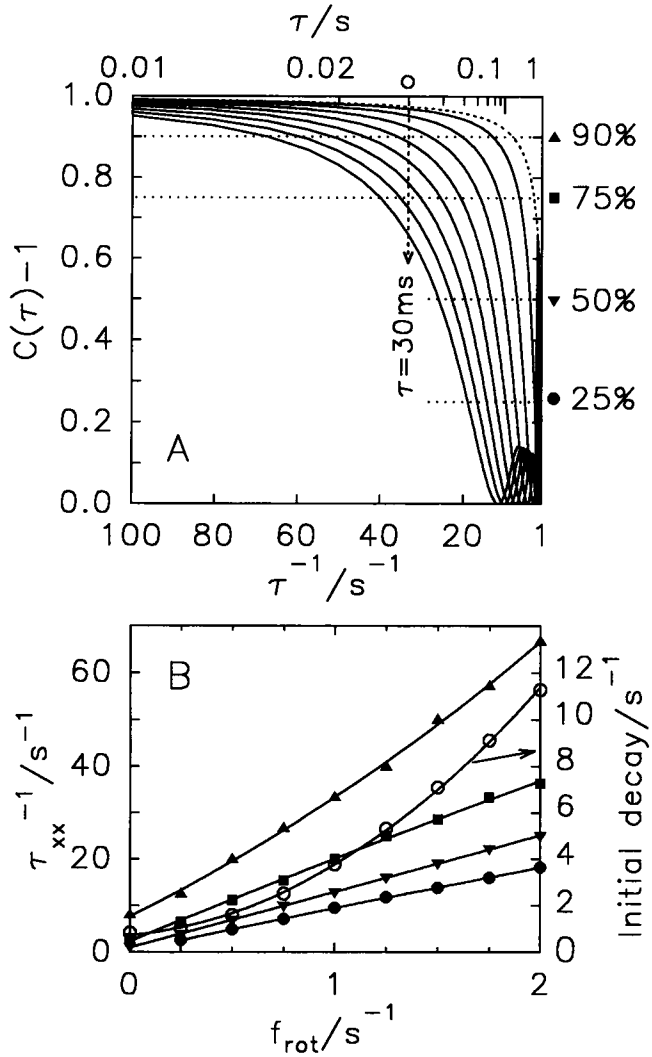

FIGURE 9 ERLS criteria applied to theoretical ACFs of a model with a radius of 3 μm, r_s = 1 μm, and a scattering angle of 10°. (*A*) Calculated ACFs for different particle rotation frequencies plotted against the inverse correlation time, $1/\tau$. The dashed line represents the control ACF with no induced rotation. The other curves represent increasing rotation frequencies up to 2 s^{-1}. The step width is 0.25 s^{-1}. The dotted horizontal lines illustrate the different decorrelation levels (decay level criteria). The initial decay for various rotation speeds is found from the intercepts with the vertical line at τ = 30 ms. (*B*) Dependence of the criteria on particle rotation frequency. Filled symbols and empty circles represent the decay level criteria marked in *A* (*left ordinate*) and the initial decay criterion for τ = 30 ms (*right ordinate*), respectively. The left ordinate is the inverse correlation time τ_{xx}^{-1} needed for the decay to the respective ACF level, xx (▲, 90%; ■, 75%; ▼, 50%; ●, 25%). The curves are polynomial regressions including the orders 0, 1, and 2.

exhibits a slight deviation. In any case, the offset is caused by the diffusional motions. The 90% criterion shows the highest offset, even relative to the value reached at 2 revolutions/s.

We favor the $1/\tau_{75}$ criterion, as it combines an almost linear dependence on rotation speed with high sensitivity for the induced rotation. It also features experimental robustness, rejecting the experimentally observed, nonreproducible ACF fluctuations at higher correlation times. The pre-

dicted linear dependence on rotation speed could be experimentally found for the $1/\tau_{75}$ criterion above a certain field strength when field frequencies close to the ER peak were used. At these frequencies cell rotation is induced with a high efficiency (Fig. 4). Additional field-induced motions result in nonlinear behavior, especially in the range of small ER speeds. These effects are not included in our model.

For the alternative initial decay criterion (the average decay of the ACF within 30 ms), an approximate quadratic dependence on particle rotation speed was found theoretically and experimentally (compare Fig. 9 B, *empty circles*, and Fig. 5 *C*). The advantage of the initial decay criterion for experiments may be a slightly higher statistical significance in the f_c determination. This was the result of nonlinear fits of the 30-ms initial decay and the $1/\tau_{75}$ criterion to the same experimental data sets.

Interpretation of ERLS control measurements

Our ERLS test measurements focus on the interpretation of the ACF in the antifield peak range. To compare the ERLS spectra to the actual ER behavior, the imaginary part of the Clausius-Mosotti function for the complete red cell model (Gimsa et al., 1996) was transformed according to the ERLS criterion used. To obtain theoretical $1/\tau_{75}$ spectra, the absolute value of the imaginary part was multiplied by a scaling factor. Then a frequency-independent offset was added. Scaling factor and offset were fitted by eye to the measuring points with the highest weight on the antifield peak range. Similarly, the initial decay values were fitted, except that the square of the imaginary part was used. The results are given by the solid lines in Fig. 5, *B* and *C*, allowing a comparison of the actual ER behavior and ERLS spectra. The characteristic frequencies of 160 and 162 kHz determined by nonlinear fits for the antifield peak from the $1/\tau_{75}$ and the initial decay criterion, respectively (see results and dotted lines in Fig. 5, *B* and *C*), are about 8% too high compared to predictions from the dielectric cell model (Fig. 5 *A*). Reasons for this may be the influence of dielectrophoretic particle movement and the dielectrophoretic cell-cell attraction on the ERLS spectra. The dielectrophoretic behavior of red blood cells at our external conductivity is characterized by two major dispersions (see Fig. 5 *A*). They mediate the transition from negative to positive DEP plateaus, where the cell is repelled and attracted by areas of high fields, respectively. At the critical frequencies, polarizability of cell and medium balance and the dielectrophoretic movement ceases. In contrast, the cell-cell attraction is caused by the interaction of the induced dipole moment of two neighboring cells. Its frequency dependence can be described by the square of the induced dipole moment of the particle (see Fig. 5 *A*). It exhibits no zero points and strongly depends on the interparticle distance (Zhelev et al., 1991).

Independent of the criterion, a small depression around 100 kHz can be seen, which is especially pronounced for the $1/\tau_{25}$ criterion (Fig. 5 *D*). For the single-shell model it is known that the first critical frequency of DEP is $2^{-0.5}$ smaller than the first characteristic frequency of ER (Gimsa et al., 1991b), rendering the first critical frequency at about 100 kHz. Around this frequency the contribution of dielectrophoretic cell movement to the ERLS spectra is minimized. Because the dielectrophoretic contribution is similar for the other frequencies, the 100-kHz data points were ignored for more consistent spectra fits. These fits yielded characteristic frequencies of 151 ($1/\tau_{75}$ criterion) and 149 kHz (initial decay criterion). These values differ by less than 1% from the model values. This also suggests that the influence of cell-cell attraction is negligibly small at our low cell concentration.

ERLS measurement of nystatin influence

When the first characteristic frequency was followed under the influence of 10 μg/ml nystatin, a clear shift to lower frequencies could be found. It is caused by a drastic decrease in the internal cytoplasmatic conductivity by ion loss and a parallel decrease in ion mobility (Gimsa et al., 1994). The control cells without nystatin showed no significant shift. This behavior is in agreement with microscopic control measurements. Nevertheless, the deviation of about 20% for the f_c of control cells is too large to determine exact parameters from one run. This problem may be overcome by longer measuring times, but this is not practicable for following the time dependence under the influence of nystatin. In addition, we were not able to clearly separate the effects of rotation speed changes and nystatin-induced cell shape transformations. Such shape transformations, by changing the optical structure of the particles, may even cause a higher sensitivity of ERLS (see increased $1/\tau_{75}$ values of the 12-min spectrum compared to 2 min for 10 μg/ml nystatin in Fig. 6). However, for a given cell shape, the ER spectra can clearly be deduced from the ERLS spectra. Moreover, the decrease in rotation speed can be followed (Fig. 6; spectra for 12, 22, and 32 min at 10 μg/ml nystatin).

From the spectra obtained at 20 μg/ml nystatin, two limitations of ERLS in our experimental situation can be seen: although microscopic measurements showed that cells still rotated at about 1 revolution/5 s 12 min after suspension, ERLS spectra showed no significant frequency dependence. Obviously such small rotation speeds can hardly be detected. A time limit of the method can be seen in the spectrum observed from 2 to 5 min after suspension. The decrease in rotation clearly occurred during measurement of the spectrum. Our procedure of experimental observation of f_c requires that changes be much slower than the recording time of one spectrum every 3 min.

CONCLUSION

Our new method of ERLS allows the expansion of laser optical particle characterization to inherent particle proper-

ties, such as internal conductivity and membrane capacitance of cells. Nevertheless, some problems remain. A deviation from perfect optical rotational symmetry is essential for ERLS detection (as for microscopic measurements), although this problem may possibly be overcome by labeling. Our optical particle model should only be considered as a first step. Up to now, the rotation sense cannot be detected. This information must be additionally obtained from microscopic control measurements, because it is essential for the characterization of dispersion processes. We propose criteria that allow us to determine the frequency dependence of the particle rotation speed from the obtained ACFs. Our criteria depend not only on the rotation speed, but also on particle shape and translational motions due to DEP and particle-particle attraction. As a result, rotation speeds significantly lower than 1 revolution/s cannot clearly be detected with red blood cells. For cell rotations faster than 1 revolution/s, ER clearly dominates the ERLS spectra, allowing the determination of characteristic frequencies of ER. ERLS measurements require optimization of particle concentration because particle concentration influences multiscattering, heterodyne rate, particle-particle interaction, and aggregation. Nevertheless, ERLS overcomes the disadvantages of tedious microscopic measurements by computerization of ER. Registration of the ACF of a particle ensemble allows statistical significance at short measuring times. These features of ERLS open the field of nonbiological applications, e.g., the study of colloidal particles. We hope that the use of DLS will be a significant breakthrough in the application of dielectric particle spectroscopy techniques.

We thank Dr. Th. Schnelle for providing the theoretical cell spectra. Ms. S. Camacho and Dr. S. G. Shirley are acknowledged for help with the manuscript.

This work was supported by DFG grants Gi 232/1-1 and Gi 232/1-2.

REFERENCES

Arnold, W. M., and U. Zimmermann. 1982. Rotating-field-induced rotation and measurement of the membrane capacitance of single mesophyll cells of *Avena sativa*. *Z. Naturforsch.* 37c:908–915.

Asami, K., Y. Takahashi, and S. Takashima. 1989. Dielectric properties of mouse lymphocytes and erythrocytes. *Biochim. Biophys. Acta.* 1010: 49–55.

Asami, K., and T. Yamaguchi. 1992. Dielectric spectroscopy of plant protoplasts. *Biophys. J.* 63:1493–1499.

Bao, J. Z., C. C. Davis, and R. E. Schmukler. 1993. Impedance spectroscopy of human erythrocytes: system calibration and nonlinear modeling. *IEEE Trans. Biomed. Eng.* 40:364–378.

Berne, B. J., and R. Pecora. 1976. Dynamic Light Scattering. Wiley, New York.

Donath, E., V. Pastushenko, and M. Egger. 1990. Dielectric behavior of the anion-exchange protein of human red blood cells: theoretical analysis and comparison to electrorotation data. *Bioelectrochem. Bioenerg.* 23: 337–360.

Engström, K. G., B. Möller, and H. J. Meiselman. 1992. Optical evaluation of red blood cell geometry using micropipette aspiration. *Blood Cells.* 8:241–258.

Eppmann, P., J. Gimsa, B. Prüger, and E. Donath. 1996. Dynamic light scattering from oriented, rotating particles: a theoretical study and comparison to electrorotation data. *J. Phys. III France.* 6:421–432.

Fuhr, G., R. Glaser, and R. Hagedorn. 1985. Rotation of dielectrics in a rotating electric high-frequency field. *Biophys. J.* 49:395–402.

Fuhr, G., U. Zimmermann, and S. G. Shirley. 1996. Cell motion in time-varying fields: principles and potential. *In* Electromanipulation of Cells. U. Zimmermann and G. A. Neil, editors. CRC Press, Boca Raton, FL. 259–328.

Georgiewa, R., E. Donath, J. Gimsa, U. Löwe, and R. Glaser. 1989. AC-field-induced KCl leakage from human red blood cells at low ionic strengths—implications for electrorotation measurements. *Bioelectrochem. Bioenerg.* 22:255–270.

Gimsa, J., R. Glaser, and G. Fuhr. 1991a. Theory and application of the rotation of biological cells in rotating electric fields (electrorotation). *In* Physical Characterization of Biological Cells. W. Schütt, H. Klinkmann, I. Lamprecht, and T. Wilson, editors. Verlag Gesundheit, Berlin. 295–323.

Gimsa, J., P. Marszalek, U. Löwe, and T. Y. Tsong. 1991b. Dielectrophoresis and electrorotation of neurospora slime and murine myeloma cells. *Biophys. J.* 60:749–760.

Gimsa, J., T. Müller, Th. Schnelle, and G. Fuhr. 1996. Dielectric spectroscopy of single human erythrocytes at physiological ionic strength: dispersion of the cytoplasm. *Biophys. J.* 71:498–506.

Gimsa, J., B. Prüger, P. Eppmann, and E. Donath. 1995. Electrorotation of particles measured by dynamic light scattering—a new dielectric spectroscopy technique. *Colloids Surf. A.* 98:243–249.

Gimsa, J., Th. Schnelle, G. Zechel, and R. Glaser. 1994. Dielectric spectroscopy of human erythrocytes: investigations under the influence of nystatin. *Biophys. J.* 66:1244–1253.

Jones, T. B. 1995. Electromechanics of Particles. Cambridge University Press, Cambridge, New York, Melbourne.

Kakutani, T., S. Shibatani, and M. Sugai. 1993. Electrorotation of nonspherical cells: theory of ellipsoidal cells with an arbitrary number of shells. *Bioelectrochem. Bioenerg.* 31:131–145.

Miller, R. D., and T. B. Jones. 1993. Electro-orientation of ellipsoidal erythrocytes. Theory and experiment. *Biophys. J.* 64:1588–1595.

Müller, T., L. Küchler, G. Fuhr, T. Schnelle, and A. Sokirko. 1993. Dielektrische Einzelzellspektroskopie an Pollen verschiedener Waldbaumarten—Charakterisierung der Pollenvitalität. *Silvae Genet.* 42: 311–322.

Ostrowski, N. 1993. Liposome size measurements by photon correlation spectroscopy. *Chem. Phys. Lipids.* 64:45–56.

Pastushenko, V. Ph., P. I. Kuzmin, and Yu. A. Chizmadshev. 1985. Dielectrophoresis and electrorotation: a unified theory of spherically symmetrical cells. *Stud. Biophys.* 110:51–57.

Paul, R., and M. Otwinowski. 1991. The theory of the frequency response of ellipsoidal biological cells in rotating electrical fields. *J. Theor. Biol.* 148:495–519.

Pauly, H., and H. P. Schwan. 1966. Dielectric properties and ion mobility in erythrocytes. *Biophys. J.* 6:621–639.

Pecora, R. 1985. Dynamic Light Scattering—Application of Photon Correlation Spectroscopy. Plenum Press, New York.

Sauer, F. A., and R. N. Schlögl. 1985. Torques exerted on cylinders and spheres by external electromagnetic fields: a contribution to the theory of field-induced cell rotation. *In* Interactions between Electromagnetic Fields and Cells. A. Chiabrera, C. Nicolini, and H. P. Schwan, editors. Plenum Publishing, New York. 203–251.

Sukhorukov, V. L., and U. Zimmermann. 1996. Electrorotation of erythrocytes treated with dipicrylamine: mobile charges within the membrane show their "signature" in rotational spectra. *J. Membr. Biol.* 153: 161–169.

Zhelev, D. V., P. I. Kuzmin, and D. S. Dimitrov. 1991. The force of mutual cell attraction induced by radio frequency electric fields. *Bioelectrochem. Bioenerg.* 26:193–203.